This article has been accepted for publication in a future issue of this journal, but has not been fully edited. Content may change prior to final publication. Citation information: DOI 10.1109/TNSRE.2014.2375879, IEEE Transactions on Neural Systems and Rehabilitation Engineering

Decoding Three-Dimensional Trajectory of Executed and Imagined Arm Movements from Electroencephalogram Signals

Jeong-Hun Kim, Felix Bießmann, and Seong-Whan Lee, *Fellow, IEEE*

***Abstract*—Decoding motor commands from non-invasively measured neural signals has become important in brain-computer interface (BCI) research. Applications of BCI include neurorehabilitation after stroke and control of limb prostheses. Until now, most studies have tested simple movement trajectories in two dimensions by using constant velocity profiles. However, most real-world scenarios require much more complex movement trajectories and velocity profiles. In this study, we decoded motor commands in three dimensions from electroencephalography (EEG) recordings while the subjects either executed or observed/imagined complex upper limb movement trajectories. We compared the accuracy of simple linear methods and non-linear methods. In line with previous studies our results showed that linear decoders are an efficient and robust method for decoding motor commands. However, while we took the same precautions as previous studies to suppress eye-movement related EEG contamination, we found that subtracting residual electro-oculogram (EOG) activity from the EEG data resulted in substantially lower motor decoding accuracy for linear decoders. This effect severely limits the transfer of previous results to practical applications in which *neural* activation is targeted. We observed that non-linear methods showed no such drop in decoding performance. Our results demonstrate that eye-movement related contamination of brain signals constitutes a severe problem for decoding motor signals from EEG data. These results are important for developing accurate decoders of motor signal from neural signals for use with BCI-based neural prostheses and neurorehabilitation in real-world scenarios.**

***Index Terms*—BCI, Arm movement trajectory, EEG, Upper limb rehabilitation, Kernel ridge regression.**

I. Introduction

BRAIN-COMPUTER interfaces (BCIs) can be used to convert electrical activity from the brain into motor control commands. Extracting commands directly from brain activity is essential for applications such as neurorehabilitation or for exerting control over limb prostheses. The best accuracy of decoding motor commands can be achieved by using invasive recordings of neural activity. Invasive BCIs have been shown to enable successful decoding of hand movement speed and direction [1] - [3] and to specifically allow the use of a prosthetic arm during fine motor control tasks such as self-feeding in experiments on non-human primates [1]. Additionally, invasive BCIs have been utilized to control robotic arms for use in human patients with tetraplegia [2], [3]. Application of invasive BCIs in humans, however, has severe disadvantages. Most importantly, invasive recordings require surgeries on the open brain, which can expose patients to inflammatory risks in the central nervous system. These risks can be avoided by obtaining non-invasive neural measurements.

Non-invasive BCIs are often based on electroencephalogram (EEG) recordings. To extract motor commands from EEG signals, several paradigms have been established. One popular paradigm involves instructing subjects to imagine right and left hand movements. Differential activation of brain regions associated with the motor control of these respective body parts can then be decoded from EEG signals [4], [5]. Motor imagery (MI) can be extended to a vast array of applications. For example, A. J. Doud et al. have successfully controlled a virtual helicopter by using sensorimotor rhythms (SMRs) induced by motor imagination [6]. Additionally, G. R. Muller-Putz et al. have shown that temporal coding of individual MI patterns can be used to control two independent degrees of an artificial robotic arm [7]. However, MI requires a large amount of calibration data and does not work for all subjects. Moreover, by using MI with body parts such as the foot or tongue to control a robotic arm or a prosthetic device is somewhat non-natural behavior. Another method to extract motor control commands from EEG signals is to use selective attention such as P300 potentials or steady state visually evoked potentials (SSVEP) [8]. While this approach is advantageous in that it requires very little training time, it is not the most intuitive method of controlling prosthetic devices and can prove difficult when targeting specific motor regions during neurorehabilitation. Moreover, SSVEP-based BCIs are based on sensory stimulation, and thus, require fixation on the stimulus that can lead to, and be affected by, eye fatigue.

Most of the above-mentioned approaches share a common disadvantage in that they do not allow direct extraction of continuous movement kinematics. In other words, the discussed approaches do not directly obtain motor signals from cortical areas that are responsible for encoding motor activity. For example, SSVEP-based BCIs require attentional modulation of sensory areas, while motor imagery-based BCIs often use motor imagery of arbitrary body parts, and not the ones that correspond to a prosthetic effector. For both applications, to

A preliminary version of this paper has been presented in the Fifth International Brain-Computer Interface Meeting, Pacific Grove, California, USA, June 2013.

This work was supported by the National Research Foundation of Korea (NRF) grant funded by the Korea government (No. 2012-005741). S.-W. Lee is corresponding author.

J.-H. Kim, F. Bießmann, and S.-W. Lee are with the Department of Brain and Cognitive Engineering, Korea University, Anam-dong, Seongbuk-ku, Seoul 136-713, Korea. E-mail: {jeonghun_kim, biessmann, sw.lee}@korea.ac.kr.

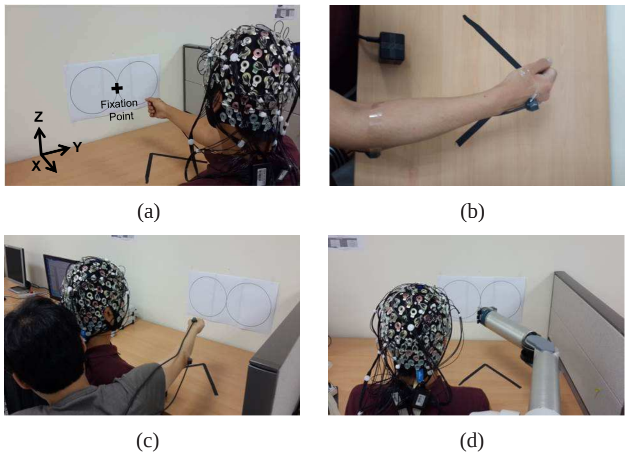

Fig. 1. Experimental setup. (a) A subject was instructed to move his arm in the shape of the infinity symbol. (b) Movement guidelines at the x-y axes. (c) Motor imagery with a volunteer's arm. (d) Motor imagery with a robotic arm.

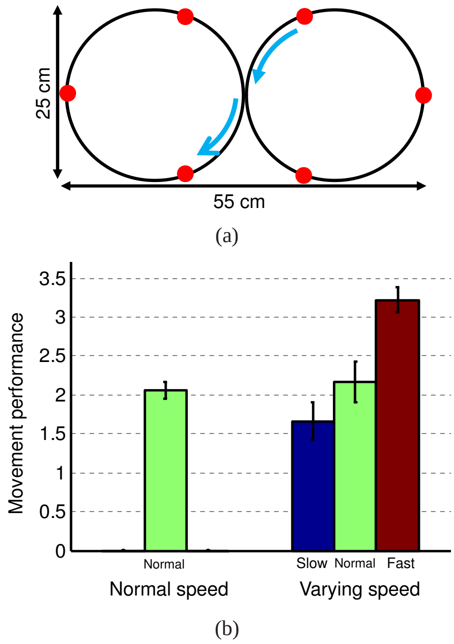

Fig. 2. (a) Electroencephalography (EEG) and motion tracking data were synchronized at the dot during arm movements. (b) Subjects' performances (average and standard derivation) of motor executions during each run. The y-axis indicates the number of arm movements per 7 s along an infinity-symbol-shaped trajectory.

achieve intuitive and accurate control of prosthetic devices as well as to attain neurorehabilitation, it is desirable to directly extract movement kinematics from the associated brain regions.

Multiple studies have shown that the low-frequency component of EEG signals in motor regions carries information about movement onset [9], direction, and velocity [10]-[14]. This has allowed several investigators to decode kinematics of the ankle, knee, and hip joints during human treadmill walking [15]. In another study, the authors were able to reconstruct hand movement velocity during a four-directional drawing task [16]. Additionally, Bradberry et al. have been able to decode 3D hand trajectories during center-out reaching tasks [10], while P. Ofner et al. proposed a new paradigm without external targets to successfully decode continuous and self-paced movements [13].

Interestingly, EEG-based studies on upper limb motor control have only focused on hand movement trajectories; however, motor control of other joints such as the elbow is also important for motor rehabilitation. When patients are trained using an effector-based robot-assisted rehabilitation system, they often lack supervision to verify whether the movements are performed in the correct manner. To this end, it is useful to assess the kinematics of the different joints of the arm. In turn, monitoring of the neural correlates of these joints, and eventual discrepancies with the observed behavior, can be useful to better understand and assist motor neurorehabilitation [14]. By using a novel preprocessing method and sparse linear regression, Y. Nakanishi et al. have predicted 3D arm and elbow trajectories over time from electrocorticography (ECoG) signals in humans [17]. To the best of our knowledge, this method has not been used to investigate whether EEG-based systems can decode upper limb motor signals other than those of hand trajectories. Therefore, in the current study we applied well-established linear decoding methods to extract the kinematics of both hand and elbow movements, when the subjects either performed a trajectory themselves or observed and imagined a trajectory performed by another entity.

To date, most studies have only decoded actual hand movement velocities. In this study, we aimed to decode 3D trajectories of imagined arm movements from EEG signals during a task that required the subjects to imagine and observe movements performed by a robotic arm or another individual's arm. Previous studies have already successfully demonstrated a similar approach [2], [11]. However, in contrast to EEG studies that focus on simple motion trajectories in 2D, here, we investigated the extent to which linear decoding methods could be used in further realistic settings. Specifically, we aimed to investigate the motor commands that were required for performing complex trajectories in 3D with varying velocity profiles.

Many previous studies have used linear methods for decoding hand kinematics. To the best of our knowledge, it has not yet been systematically explored whether non-linear methods can yield better results when decoding arm trajectories by using EEG signals. Therefore, in the current study we compared the results of linear methods with decoding accuracies obtained using a non-linear method.

To enhance the performance of EEG-based BCIs, several studies have explored additional sources of control commands outside neural activation. For example, G. Onose et al. used eye tracking to provide motion end-point information to a robotic arm by inferring the location of the object to be grasped from the focus point of a gaze that was concurrent with motor imagination [18]. However, the additional measurement device used in these studies can cause discomfort and increase cost. More importantly, for the therapeutic goal of neurorehabilitation to be accomplished, it is essential that *only* neural motor commands be used. In this study, we

This article has been accepted for publication in a future issue of this journal, but has not been fully edited. Content may change prior to final publication. Citation information: DOI 10.1109/TNSRE.2014.2375879, IEEE Transactions on Neural Systems and Rehabilitation Engineering

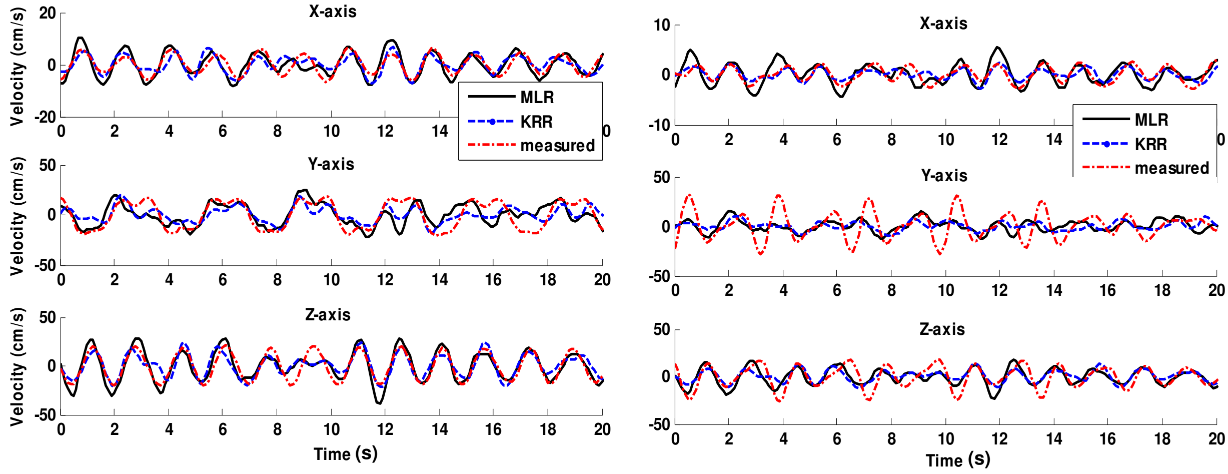

(a) (b)

Fig. 3. Decoder example of executed arm movements: The comparison between the measured velocity (red dotted line) and decoded velocity (kernel ridge regression [KRR]: blue dotted line; multiple linear regression [MLR]: black solid line) from subject 1 in the time domain. (a) Hand movements at normal velocity. (b) Elbow movements at normal velocity.

aimed to assess how eye movements affect decoding of neural motor signals in complex real-world scenarios. The eye is a much stronger dipole than that of the neural sources in the brain. Consequently, any eye movement that is correlated with motor commands (eye-stabilizing reflexes during head or body movement or eye movement when pursuing a target in a motor task) will be reflected in an EEG. Because of volume conduction, eye movement-related signals will not only be reflected in electrodes close to the eye but also in distant electrodes. Therefore, for BCIs and neurorehabilitation, it is critical that eye-related signals are excluded from motor decoding. In most previous studies subjects were instructed to suppress eye movements. During the session eye movements were monitored by the experimenter and electro-oculogram (EOG) activity was measured. EOG contamination of EEG activity is then measured by correlating the labels (i.e. movement velocity of the controlled limb) with the EOG activity [11]. Low correlations around 0.1 are then interpreted as EEG being not contaminated by EOG activity. Note however that this procedure does not ensure that the decoder does not use EOG related signals, whether or not they are volitionally or subconsciously following the target position. Even if the EOG activity is not correlated to the target signal, correlations of EEG activity with this non-neural noise source can be used by the decoder to improve noise subtraction. Other studies used gaze tracking to ensure that there are no eye movements that could contaminate the EEG. However gaze trackers cannot detect eye movements such as rotations around the rostro-caudal (roll) axis, which will lead to EEG contaminations. Here we provide empirical evidence for such undetected EOG contamination of EEG signals in motor decoding tasks, see e.g. Fig. 6. While we took the same precautions previous studies to suppress eye movement, we found that removing residual eye-movement related artifacts in neural measurements can substantially decrease motor decoding accuracy when using standard linear methods. Moreover we found that non-linear decoding methods can help to counteract this loss in decoding accuracy. We hope that our results can raise awareness for the problem of EEG signal contamination by eye movements in motor signal decoding from neural signals and can help to improve motor signal decoding systems operating under realistic experimental conditions.

II. Materials and Methods

A. Experimental Procedure

Ten healthy right-handed male subjects between the ages of 25 and 32 years participated in this experiment. The subjects were seated in an armchair for the duration of the study. The experiment consisted of three sessions where the subjects were asked to execute a motor trajectory (first session) (Fig. 1(a)), observe the trajectory performed by a volunteer's hand and imagine the motor command for this trajectory (second session) (Fig. 1(c)), and to observe a trajectory performed by a robotic arm and imagine the movement associated with it (third session) (Fig. 1(d)). Each session comprised of two runs, one with a constant movement velocity profile and a second run with varying movement velocity profile. In each run, the subjects were asked to perform eight trials of motor execution or imagination. Each trial lasted 60 s, with the start of a trial being indicated using a short tone; defined breaks were set between trials to avoid fatigue.

In each trial, the subjects were instructed to execute or imagine a movement trajectory in the shape of an infinity (∞) symbol and a "$\wedge$" symbol when viewed from y-z axes and x-y axes, respectively (Fig. 1(a), 1(b)). The subjects were also directed to synchronize their arm movement speed by using a metronome. In the constant velocity profile session, the interval between two metronome ticks was 1700 ms. The subjects were asked to complete one-half of the infinity symbol with each metronome tone. After two metronome clicks, the subjects were to have moved their hand once around the specified trajectory. In the first run, the subjects moved their arm at normal speed; thus, during this condition, the

This article has been accepted for publication in a future issue of this journal, but has not been fully edited. Content may change prior to final publication. Citation information: DOI 10.1109/TNSRE.2014.2375879, IEEE Transactions on Neural Systems and Rehabilitation Engineering

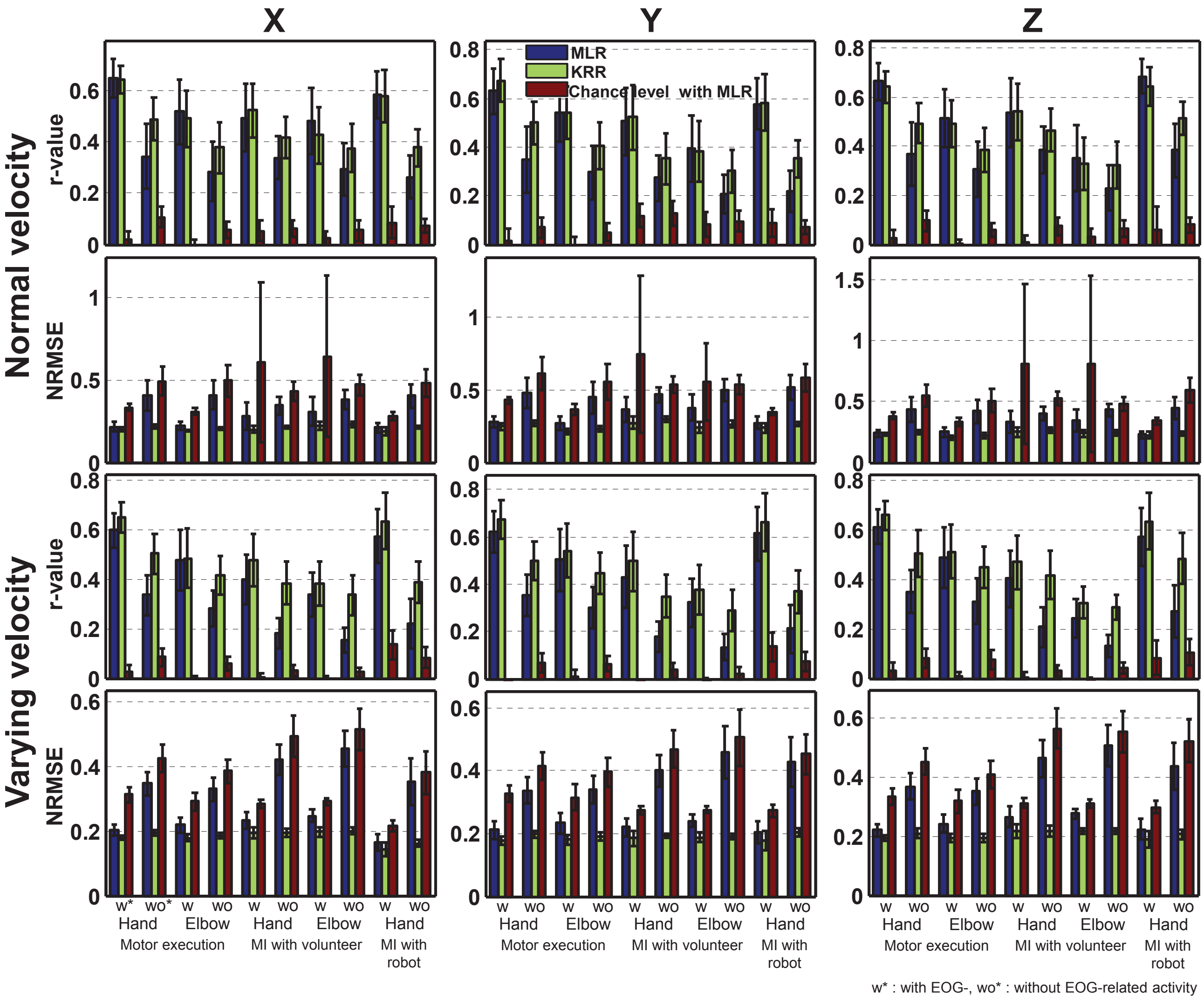

Fig. 4. Movement trajectory decoding performance on holdout data for linear (multiple linear regression [MLR], blue) and non-linear (kernel ridge regression [KRR], red) decoders. Each column shows the results for x-, y-, and z-directions, respectively. The performance measured in correlation and normalized root-mean-square errors (NRMSEs) between measured and predicted trajectories are plotted for constant velocity profile and varying velocity profile conditions.

variation of the hand velocity was low. In the second varying velocity profile session, the metronome ticks were paced at 1000 ms, 1700 ms, and 2400 ms intervals, with the speed of the metronome changing every 7 s. The volume of the metronome was kept low to reduce the effects on brain signals. To reduce eye movement-related artifacts, the subjects were asked to fix their eyes on a cross that was located in the middle of a vertical plane (Fig. 1(a)). The robotic arm (WAM arm, Barrett technology, Fig. 1(d)) was controlled using a ”teach and play” function that involved us recording eight trial trajectories before the experiment that corresponded to the constant velocity and varying velocity profiles. The recorded trajectories were then used for the third session (introduced above) of the experiment.

B. Data Collection

For EEG data collection, a BrainAmp system (Brain Products GmbH, Germany) was utilized, along with 64 integrated electrodes arranged in the modified 10/20 international system, with the ground on FPz and reference placed on FCz. Vertical and horizontal EOG activity was also recorded. Electromyographic (EMG) signals were amplified and collected from two bipolar surface electrodes over the flexor carpi radialis and extensor digitorum muscles of the right forearm [11] during the imagery sessions. EEG, EOG, and EMG signals were acquired using a sampling frequency of 1 kHz.

Three-dimensional hand and elbow positions were recorded using a motion-tracking device (FASTRAK, Polhemus) at a sampling rate of 60 Hz. The tracking device was attached to the hands and elbows of the subjects during the first session and was then switched to the volunteer for the second session. Both EEG and motion tracking data for analysis were synchronized using a computer.

For the third session, the robotic arm was controlled using a computer with the arm’s 3D position being recorded at a sampling rate of 1 kHz. Both EEG and robotic arm data were synchronized for analysis.

To investigate a subject’s performance movement according

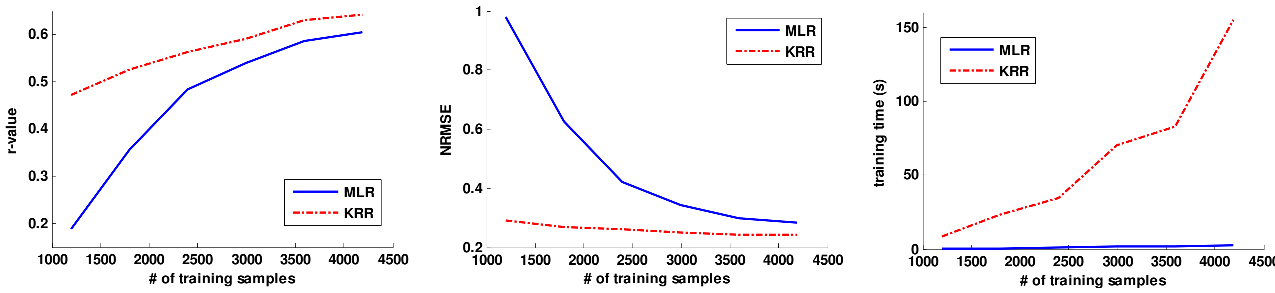

(a) (b) (c)

Fig. 5. Decoding performance and computational cost as a function of the number of training samples for different decoders. Decoding performance, as measured using r-value (*a*) or normalized root-mean-square error (NRMSE) (*b*) increased with the amount of training data. While the training time of linear models was small even for a large training data set, the training time for the non-linear kernel ridge regression model increased exponentially with the number of data points (*c*).

to the metronome, the infinity symbol was divided into six areas (Fig. 2(a)). When a subject moved his hand to the next division of the symbol, EEG and motion tracking data were synchronized for analysis by using a computer.

C. Signal Preprocessing

Continuous EEG signals were down-sampled to 100 Hz. To investigate the effect of EOG activity on decoding performance, we used two types of preprocessed EEG data: EEG signals with EOG-related activity removed and EEG signals with EOG-related activity included. To extract EOG-related activity, we used a similar approach as reported in a previous study [19]. Briefly, we computed independent component analysis (ICA) for all EEG electrodes (EOG electrodes were excluded) by using temporal decorrelation source separation (TDSEP) algorithm [20]. Prior to performing the ICA, we reduced the dimensionality of the EEG data by using principal component analysis (PCA) to retain the minimum number of principal components needed to explain 99.9% of the variance in the data. On the remaining principal components, we computed the ICA and the correlation between each independent component with all EOG channels. Fig. 6 shows examples of EOG contamination tests used in previous studies and the correlations of ICs with EOG channels. A correlation coefficient of more than two standard deviations (0.4) away from the mean correlation coefficient was determined as a conservative threshold to reject ICs as EOG contaminated. ICs with EOG correlations of more than 0.4 we considered to be related to eye-movement rather than to neural activity. Note however that complete removal of eye-movement related activity is difficult. We here aimed at a removal method that is both efficient and simple to implement[1]. Although the linear artifact removal is potentially limited, it is a first step towards better non-invasive neural decoders in motor control. We then projected the data back into the EEG source space by using the mixing matrix that was obtained from the ICA.

The EEG signals were band-pass filtered from 0.1 to 40 Hz and then a zero-phase, fourth-order, low-pass Butterworth filter with a cutoff frequency of 1 Hz was applied to the EEG and kinematic data. The continuous EEG data were then segmented into trials. Next, we computed the temporal difference of the EEG activity as in a previous study [10], and data from each EEG sensor were standardized according to equation (1).

$$S_n[t] = \frac{v_n[t] - \mu_{v_n}}{\sigma_{v_n}} \tag{1}$$

where $S_n[t]$ and $v_n[t]$ are the standardized and differenced voltage at sensor n at time t, μ_{v_n} and σ_{v_n} are, respectively, the mean and SD of v_n, and n is the number of sensors.

D. Decoding Model

We employed two different approaches to decode arm movement velocity: the multiple linear regression (MLR) that had been used in a previous study and the kernel ridge regression (KRR).

In the MLR, we used a linear model similar to that used in a previous study [10]. The model is described in equations (2) - (4).

$$x[t] - x[t-1] = a_x + \sum_{n=1}^{N}\sum_{k=0}^{L} b_{nkx} S_n[t-k] \tag{2}$$

$$y[t] - y[t-1] = a_y + \sum_{n=1}^{N}\sum_{k=0}^{L} b_{nky} S_n[t-k] \tag{3}$$

$$z[t] - z[t-1] = a_z + \sum_{n=1}^{N}\sum_{k=0}^{L} b_{nkz} S_n[t-k] \tag{4}$$

where $x[t] - x[t-1], y[t] - y[t-1]$, and $z[t] - z[t-1]$ are the velocities at time t in the x, y and z axis. L(=10, corresponding to 100ms) is the number of time lags, $S_n[t-k]$ is the standardized difference in voltage measured at EEG sensor n at time lag k, and the a and b variables are weights obtained through multiple linear regression. N is the number of electrodes used in analysis.

Besides the well-established linear decoding method, we explored a generic non-linear decoding model by utilizing the KRR, an approach that is equivalent to the mean of a Gaussian process regression, which is a very popular method used for

[1] Note that using linear methods to discard EOG contamination we cannot exclude that there are residual non-linearly transformed EOG signals present in the EEG data. Unfortunately to the best of our knowledge there are no robust non-linear artifact removal procedures for the present application;

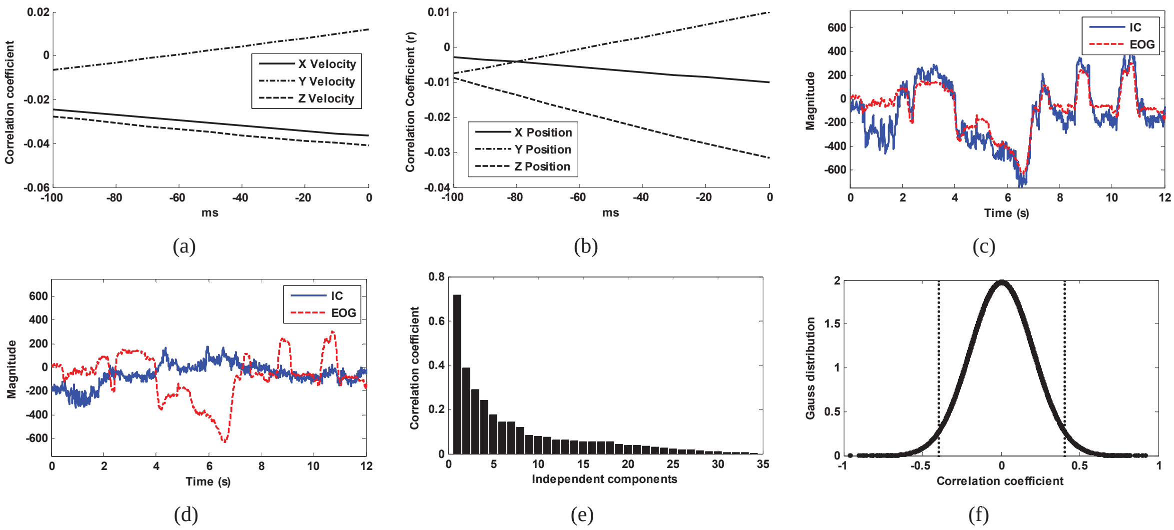

Fig. 6. (*a* and *b*): EOG contamination tests used in previous studies were based on the cross-correlogram between the EOG channels and the target variable. Also in our experiments, these correlations were diminishingly low as shown in the cross-correlogram for subject 1 in panel (*a* and *b*); panel (*c*) shows an example of horizontal EOG channel activity and a correlated independent component (IC), which was removed from the data; (*d*) shows the same EOG activity and an example of an uncorrelated IC, which was not removed. (*e*): Correlation coefficients (absolute values) between horizontal EOG channel activity and each IC of EEG activity in one trial of the experiment. Panel (*f*) shows the histogram of correlations between EOG and ICs for all subjects in all experiments. Mean and standard deviation are about 0.002 and 0.2. Dotted lines indicate threshold (0.4 and -0.4) for rejection of an IC from the EEG data. We rejected all ICs with a correlation coefficient that was 2 times the standard deviation away from the mean.

motor control in robotics [21]. The input data $\tilde{s}[t]$ is defined as the temporally embedded standardized EEG signal

$$\tilde{s}[t] = \begin{bmatrix} s[t-0] \\ \vdots \\ s[t-L] \end{bmatrix}, \text{ where } s[t] = \begin{bmatrix} S_1[t] \\ \vdots \\ S_N[t]. \end{bmatrix}. \quad (5)$$

The input data $\tilde{s}[t]$ is plotted through mapping ϕ onto a kernel feature space. KRR uses the kernel trick [22], [23] in order to estimate a non-linear function of the input data. A kernel function $k(.,.)$ computes the inner product of two data points in a kernel feature space.

$$k(\tilde{s}[i], \tilde{s}[j]) = \langle \phi(\tilde{s}[i]), \phi(\tilde{s}[j]) \rangle_\phi \quad (6)$$

We have used a Gaussian kernel function

$$k(\tilde{s}[i], \tilde{s}[j]) = e^{-(\tilde{s}[i]-\tilde{s}[j])^2/\sigma} \quad (7)$$

where σ is the width of the Gaussian kernel function. The kernel trick essentially makes use of the fact that we can express the optimal non-linear function ϕ^* as a linear combination of data similarities in a kernel feature space

$$\phi^*(s[i]) = \sum_j k(\tilde{s}[i], \tilde{s}[j])\alpha_j \quad (8)$$

where j is an index variable that runs over all training data $\tilde{s}(j)$ and α_j are dual coefficients that are obtained by

$$\alpha = (K + I\lambda)^{-1} \cdot V^\top. \quad (9)$$

Here I is the identity matrix, λ denotes a regularization parameter, K is the square kernel matrix computed on all training data points, so the entry K_{ij} is the output of the kernel function evaluation between training data point i and j

$$K_{ij} = k(\tilde{s}[i], \tilde{s}[j]), \quad (10)$$

and V denotes the target variable, the velocity at time t in the x, y and z axis

$$v(t) = \begin{bmatrix} x(t) - x(t-1) \\ y(t) - y(t-1) \\ z(t) - z(t-1) \end{bmatrix}, \quad (11)$$

$$V = [v(t=1), \ldots, v(t=T)]. \quad (12)$$

The predictions $\hat{y}(\tilde{s}[i])$ of KRR for a new data point $\tilde{s}[i]$ is then obtained using equation (8).

For decoding we exclude seven electrodes (Fp1, Fp2, AF7, AF3, AFz, AF4, AF8) from the analysis to further mitigate the influence of any eye movements on reconstruction [10].

E. Data Analysis

To assess the accuracy of the velocity decoder, we carried out a blockwise 8-fold cross-validation method to keep the training set and test set not only disjointed, but as independent as possible [24]. In an attempt to evaluate the decoding accuracy in the test set, we calculated two performance measures. The correlation coefficient (r-value) between measured movement velocity of the subject, volunteer, or the robotic arm, and the predicted movement velocity was used to compare the results of the current study to those of previous studies [10]. The correlation is computed by

$$r = \frac{C(x,y)}{\sqrt{C(x,x), C(y,y)}} \quad (13)$$

where $C(x,y)$ is the univariate covariance between x and y, x and y are the measured and decoded velocities along each direction in 3D space. We also computed the normalized root-mean squared error (NRMSE), which yields a more authentic

This article has been accepted for publication in a future issue of this journal, but has not been fully edited. Content may change prior to final publication. Citation information: DOI 10.1109/TNSRE.2014.2375879, IEEE Transactions on Neural Systems and Rehabilitation Engineering

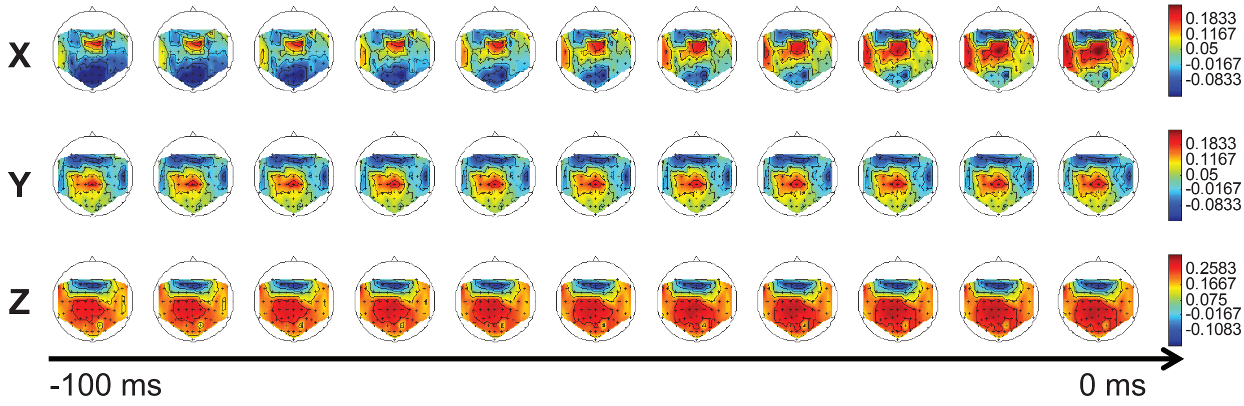

Fig. 7. Timelag of scalp maps with the correlation between standardized electroencephalography (EEG; after removal of electroocular [EOG]-related activity) and standardized arm movement velocity from subject 3 during motor execution of the hand. The 11 time series exhibited similar contributions for decoding trajectory.

estimate of the decoding performance [25]:

$$NRMSE = \frac{\sqrt{\frac{\sum_{i=1}^{n}(x_i - y_i)^2}{n}}}{x_{max} - x_{min}}. \tag{14}$$

In the current study, we used a nested cross-validation to optimize the hyperparameters of the KRR (λ, σ). In the training set, a second (inner) cross-validation was performed to determine the out-of-sample performance for a certain parameter configuration. This inner cross-validation was repeated for all parameter configurations, and the best configuration was used to train the algorithm for the outer cross-validation.

To use the decoder in clinical applications, training data is required for calibrating the decoder. Ideally, a decoder should use as little training data as possible to reduce the calibration time. We measured the decoder performance as a function of the amount of training data and reduced training samples by performing cross-validation with only 2, 3, 4, 5, 6, and 7 training blocks.

As an additional control, we shuffled each trial of EEG and motion tracking data in a training set of the same run. We then carried out 8-fold cross-validation and nested cross-validation for optimizing the parameters of the KRR to obtain an estimate of chance-level performance.

Lastly, to graphically assess the relative contributions of scalp regions to the reconstruction of executed and imagined arm velocity, we computed the the correlation between standardized EEG time series after EOG removal and the measured arm movement velocity [26]. The corresponding scalp maps are plotted in Fig. 8.

III. Results and Discussion

A. Performance Comparison Between MLR and KRR

The subjects' performance during the movement task is shown in Fig. 2(b). The executed movement velocities corresponded well to the designated velocities, indicating that the subjects reliably followed the specified infinity shape movement trajectory. For each subject, 3D arm movement velocities were decoded using MLR and KRR. The results show that both MLR and KRR can reliably decode 3D arm velocity from EEG signals. Figure 3 shows representative results obtained from a single subject during the constant velocity profile condition, while Fig. 4 shows the complete results averaged across all 10 subjects. In line with previous studies that used simple movement tasks with constant velocity profiles, we found that linear methods could decode executed movements with high accuracy [10]. Additionally, velocities of executed hand movements were decoded the most accurately from EEG signals, by using both linear and non-linear methods. Overall, we determined that movement imagined through observation of either a volunteer or a robotic arm, rather than a trajectory executed by the individual, was much more difficult to decode. Importantly, we found that the velocity profiles, both constant and varying, were reliably decoded. In the constant velocity profile condition, the decoding accuracy as measured using the correlation coefficient was not significantly different when comparing KRR and MLR; however, we determined that KRR showed higher accuracies than that by MLR as established using normalized root-mean-square error (NRMSE) (p $< 10^{-5}$). This indicates that in the constant velocity profile condition, both linear- and non-linear methods could capture the movement trajectory, but that non-linear KRR decoding showed better results when modeling the exact scaling of the desired output. On the other hand, in the varying velocity profile condition, we found that KRR showed higher decoding accuracies than that by MLR in both the r-value and NRMSE evaluations. The results suggest that non-linear methods can improve the simple linear models in complex motor tasks. We also observed that chance level decoding yielded correlation coefficients below 0.1 and 0.15 with MLR and KRR, respectively. This finding shows that decoding results obtained using both linear- and non-linear methods were well above the chance level, even in complex motion trajectory tasks.

B. Effect of Reduced Training Data

Fig. 5(a) and 5(b) show the decoding accuracy as a function of the number of training samples. We found that KRR could be used to accurately predict arm velocities by using fewer training data compared to that by using MLR. KRR showed

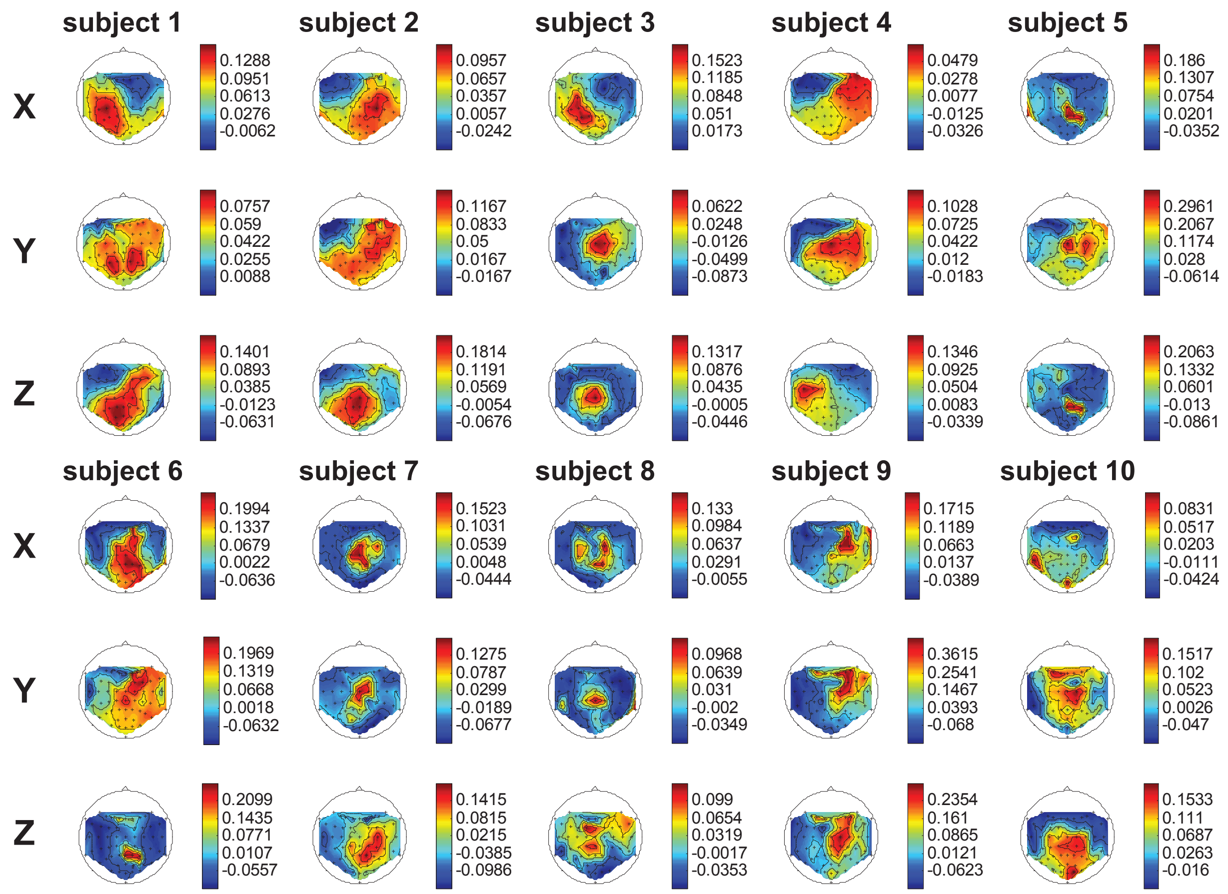

(a)

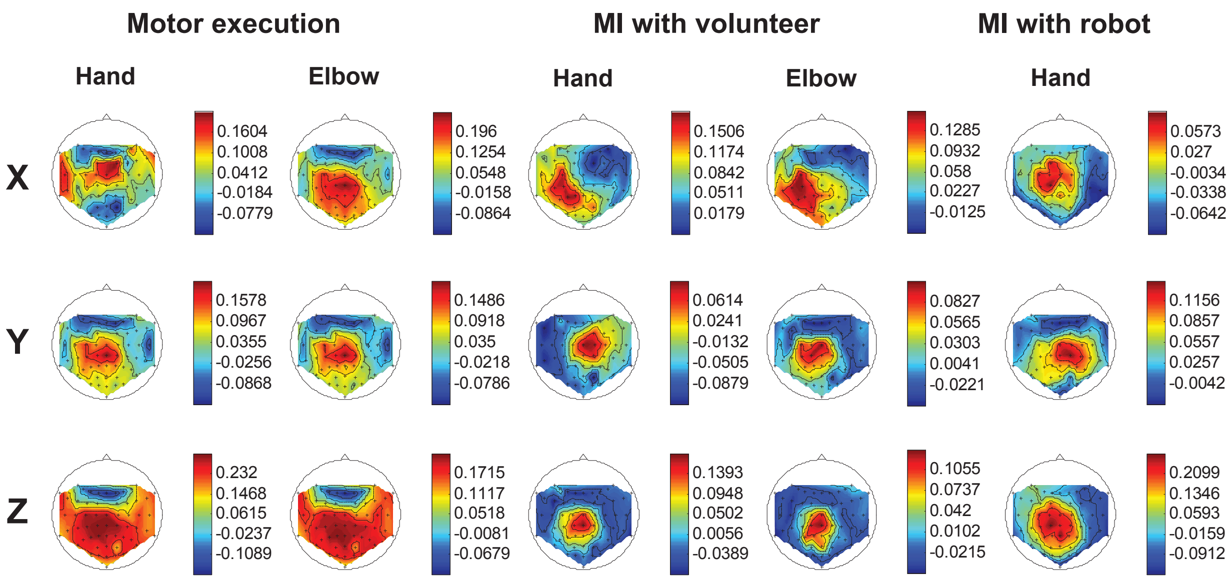

(b)

Fig. 8. Scalp maps of the correlation between standardized EEG (after removal of EOG-related activity) and standardized arm movement velocity. Seven prefrontal electrodes were excluded from the analysis. The scalp maps were at 50 ms in the past. (*a*): Scalp maps of all subjects during motor imagery with volunteer. (*b*): Scalp maps of subject 3 during all tasks.

This article has been accepted for publication in a future issue of this journal, but has not been fully edited. Content may change prior to final publication. Citation information: DOI 10.1109/TNSRE.2014.2375879, IEEE Transactions on Neural Systems and Rehabilitation Engineering

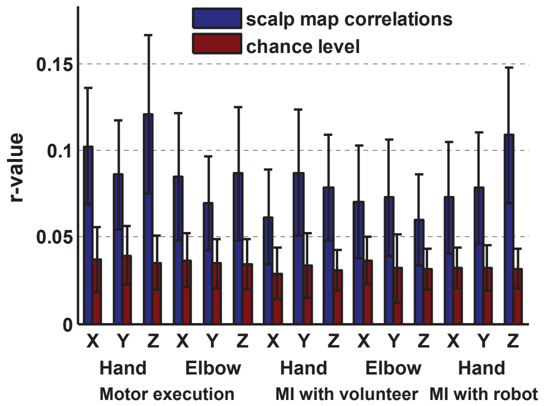

Fig. 9. Comparison of correlations plotted in fig. 8 with chance level correlations; for calculating the chance level correlations, we shuffled each trial of EEG and motion tracking data in the same run. Absolute correlation coefficients were averaged across all channels for each subject. This figure shows that scalp map correlations are above chance level.

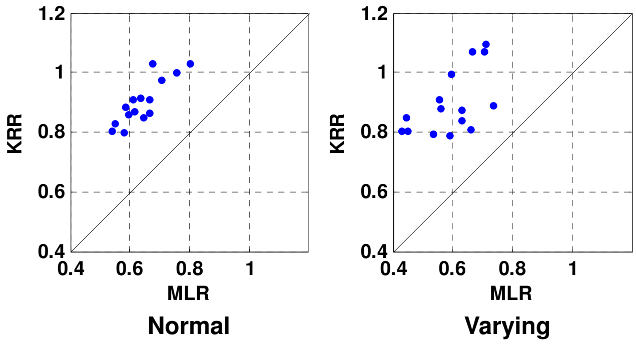

Fig. 10. Ratio between decoding accuracy after and before electroocular (EOG)-related activity from EEG signals (see Eq. 15) for linear regression (multiple linear regression [MLR], x-axis) and non-linear kernel ridge regression (kernel ridge regression [KRR], y-axis). Significantly lesser decrease in KRR decoding accuracy was observed compared to that in MLR.

NRMSE values of under 0.3 with 1200 samples, whereas MLR needed about 2800 samples to obtain a similar level of precision. Fig. 5(c) shows computation time needed for decoder training as a function of the number of training samples. Decoding with KRR reduced the error in decoding movement trajectories, but this improvement involved high computational costs. More specifically, the training time of the KRR model increased with the number of data points, which determines the size of the kernel matrix that needs to be inverted (see equation 9).

C. Effects of EOG and EMG on Decoding

To investigate the effects of EOG and EMG on decoding performance, we compared the ICA components of EEG with EOG and EMG signals. We emphasize that while we cannot ensure that all eye-movement related activity is removed from the EEG, this does not compromise the comparison. Primarily we wanted to investigate the effect of eye-movement related activity on decoding performance in real world scenarios when using different decoding models. Note that also monitoring eye movements with other techniques than EOG electrodes can fail to measure all eye movements. For instance using gaze tracking to exclude recordings does not ensure that no eye-related activity is present in the EEG, that can be used by the decoder to improve decoding accuracy. As in previous studies we found no strong correlations between EOG activity and hand movement velocity, see Fig. 6. Neither did we find any significant correlations with EMG channels in the imagined movement condition. However, some ICA components showed strong correlations with the EOG signals. Our results strongly suggest that when EOG-related activity was left in the EEG recordings, the signals were being used by the decoder. Moreover, decoding performance was found to decrease substantially once EOG-related activity was removed ($p < 10^{-5}$) (see Fig. 4). When comparing raw EEG data with the EEG data from which EOG-related activity had been removed, we found a significant drop in the decoding accuracy for the linear decoding method ($p < 10^{-5}$); however, this large drop in performance was not observed for the non-linear decoding approach. Therefore, we evaluated the strength of the effect of EOG-related activity in EEG data in both linear and non-linear decoding, by calculating the ratio of

$$\frac{Performance_{withoutEOG}}{Performance_{withEOG}}. \tag{15}$$

We then plotted the coefficients averaged across all runs per session in Fig. 10 and found that the drop in performance was substantially lower when using the non-linear decoding method. Investigating why non-linear decoding methods yielded better accuracies is an important topic of future research. One possible explanation is that motor control is a difficult problem and representing all trajectories required in realistic conditions in a linear subspace of EEG activity could not be possible. Kernel methods, as KRR used in this study, have proven very useful in previous studies for the task of motor control in robotics [21]. These results suggest that motor control of complex trajectories are better modeled using non-linear models. Besides, we cannot fully exclude that the non-linear decoder used non-neural signals in the EEG data which is not accessible to the linear decoder. We emphasize that this could explain some, not necessarily all, of the decoding accuracy differences.

D. Performance Comparison Between Hand and Elbow

We found that elbow velocity could be decoded at slightly smaller accuracy than hand velocity. This could be due to the trajectory the subjects performed. Subjects can move their hand towards the body center (along the x-axis) with smaller elbow movements in the left side of infinity symbol compared to the right side. So velocity variation and movement distance of elbow movements are different on the left and right side of the infinity symbol trajectory whereas hand movements are almost the same on both sides. This could explain some of the decoding accuracy differences. Our results show that using non-linear decoding, we could obtain higher correlation values of about 0.4 averaged across all subjects. Moreover, the scalp plots showed that hand and elbow movements elicited similar patterns of activation, which can be explained by the high correlation of direction and velocity profiles between hand and elbow movements in the task. Consequently, the correlation scalp maps of hand and elbow trajectories were similar (Fig. 8). During hand motor execution, the sensors Cz, C3 and CP2-CP3 of the modified 10/20 international system exhibited high correlations in the x and y axis. Similarly, C3, Cz, CP2-CP3 and P2-P3 were also strongly correlated with the x and y axes during motor execution of the elbow. Along the z-axis, strong correlations were observed not only in the motor cortex but also in the occipital regions. CP3 showed the highest correlation averaged across all movement axes, which is in line with findings in a previous study [10].

E. Decoding Trajectory of Imagined Arm Movement

We decoded 3D imagined hand and elbow movements during a combined task of imagination and observation of a robotic arm or a volunteer's arm. Our results show that when the subjects observed/imagined the robotic arm movement, decoding performance *with EOG related activation* was significantly higher than when subjects observed/imagined a volunteer's arm movement ($p < 10^{-5}$). However, after eliminating EOG-related activity, we found that the decoding performance of the two conditions was similar, indicating that the improved decoding accuracy in the robotic arm condition was because of eye movement-related activity rather than differences in neural activation. The robotic arm was larger and more unnatural than that of a human arm; therefore, we speculated that the high EOG-related activation was because of the difference in physical appearances between the two arms. Another possible explanation could be that another person's arm performs smoother movements and is more similar in shape to an own arm than a robotic arm; thus subjects could imagine the hand movement more easily and neural circuits such as the mirror neuron system [11] could be enhanced. Fig. 8 shows that movement velocities were highly correlated with EEG activity above motor cortex, FC1-FC4 and P1-P4.

IV. CONCLUSIONS

In the current study, we used non-invasive EEG recordings to extract motor control signals for complex 3D movement trajectories with varying velocity profiles. The experimental conditions are much closer to real-world scenarios of EEG-based BCI control for neuroprostheses or neurorehabilitation than in previous studies. We found that both executed and imagined movements could be reliably decoded from a low frequency component of EEG signals and that this was true for hand movement velocities as well as elbow velocity. Importantly, we found that in all tested conditions, the EEG activity was correlated to the EOG activity; removing the eye-related activity from EEG data resulted in a substantial drop of decoding accuracy when using the linear model. We did not observe such a strong decrease in decoding accuracy when using non-linear decoding methods. Investigating why non-linear methods perform better is an important topic of future research. To summarize, the present study showed that it is possible to decode executed and imagined complex 3D hand and elbow movement trajectories from low-frequency EEG signals. Furthermore, the results of this study could form the basis of efforts aimed to develop natural movement control of an upper limb neuroprosthesis.

ACKNOWLEDGMENT

The authors would like to thank Prof. Klaus-Robert Müller for helpful discussions and advice.

REFERENCES

[1] M. Velliste, S. Perel, M. C. Spalding, A. S. Whitford, and A. B. Schwartz, "Cortical control of a prosthetic arm for self-feeding," *Nature*, vol. 453, no. 7198, pp. 1098-1101, 2008.
[2] L. R. Hochberg, D. Bacher, B. Jarosiewicz, N. Y. Masse, J. D. Simeral, J. Vogel, S. Haddadin, J. Liu, S. S. Cash, P. v. d. Smagt, and J. P. Donoghue, "Reach and Grasp by People with Tetraplegia using a Neurally Controlled Robotic Arm," *Nature*, vol. 485, no. 7398, pp. 372-375, 2012.
[3] J. L. Collinger, B. Wodlinger, J. E. Downey, W. Wang, E. C. Tyler-Kabara, D. J. Weber, A. J. C. McMorland, M. Velliste, M. L. Boninger, and A. B. Schwartz, "High-performance neuroprosthetic control by an individual with tetraplegia," *The Lancet*, vol. 381, no. 9866, pp. 557-564, 2013.
[4] F. Galán, M. Nuttinc, E. Lew, P. W. Ferrez, G. Vanacker, J. Philips, and J. d. R. Millán, "A brain-actuated wheelchair: Asynchronous and non-invasive Brain-computer interfaces for continuous control of robots," *Clin. Neurophysiol.*, vol. 119, pp. 2159-2169, 2008.
[5] T.-E. Kam, H.-I. Suk, and S.-W. Lee, "Non-Homogeneous Spatial Filter Optimization for ElectroEncephaloGram-Based Motor Imagery Classification," *Neurocomputing*, vol. 108, no.2, pp. 58-68, 2013.
[6] A. J. Doud, J. P. Lucas, M. T. Pisansky, and B. He, "Continuous Three-Dimensional Control of a Virtual Helicopter Using a Motor Imagery Based Brain-Computer Interface," *PLoS ONE*, vol. 6, no. 10, pp. 1-10, 2011.
[7] G. R. Müller-Putz, R. Scherer, G. Pfurtscheller, and C. Neuper, "Temporal coding of brain patterns for direct limb control in humans," *Frontiers in Neuroscience*, vol. 4, no. 34, pp. 1-11, 2010.
[8] G. D. Johnson, N. R. Waytowich, D. J. Cox, and D. J. Krusienski, "Extending the Discrete Selection Capabilities of the P300 Speller to Goal-Oriented Robotic Arm Control," Proceedings of the 2010 3rd IEEE RAS and EMBS, International Conference on Biomedical Robotics and Biomechatronics, The University of Tokyo, Tokyo, Japan, pp. 572-575, 2010.
[9] E. Lew, R. Chavarriaga, S. Silvoni, and J. d. R. Millán, "Detection of Self-paced Reaching Movement Intention from EEG Signals," *Frontiers in neuroengineering*, vol. 5, pp. 1-17, 2012.
[10] T. J. Bradberry, R. J. Gentili, and J. L. Contreras-Vidal, "Reconstructing Three-Dimensional Hand Movements from Noninvasive electroencephalographic signals," *J. Neurosci.*, vol. 30, pp. 3432-3437, 2010.
[11] T. J. Bradberry, R. J. Gentili, and J. L. Contreras-Vidal, "Fast attainment of computer cursor control with noninvasively acquired brain signals," *J. Neural Eng.*, vol. 8, pp. 1-9, 2011.
[12] J. Liu, C. Perdoni, and B. He, "Hand Movement Decoding by Phase-locking Low Frequency EEG Signal," 33rd Annual International Conference of the IEEE Engineering in Medicine and Biology Society, Boston, USA, pp. 6335-6338, 2011.
[13] P. Ofner and G. R. Müller-Putz, "Decoding of Velocities and Positions of 3D Arm Movement from EEG," 34th Annual International Conference of the IEEE Engineering in Medicine and Biology Society, San Diego, USA, pp. 6406-6409, 2012.
[14] J.-H. Kim, R. Chavarriaga, J. d. R. Millán, and S.-W. Lee, "3D Trajectory Reconstruction of Upper Limb Based on EEG," Fifth International Brain-Computer Interface Meeting 2013, Pacific Grove, California, USA, Jun., 2013.
[15] A. Presacco, R. Goodman, L. Forrester, and L. Contreras-Vidal, "Neural decoding of treadmill walking from noninvasive electroencephalographic signals," *J. Neurophysiol.*, vol. 106, pp. 1875-1887, 2011.
[16] J. Lv, Y. Li, and Z. Gu, "Decoding Hand Movement Velocity from electroencephalogram Signals during a Drawing Task," *BioMedical Engineering Online*, vol. 9, no. 64, pp. 1-21, 2010.
[17] Y. Nakanishi, T. Yanagisawa, D. Shin, R. Fukuma, C. Chen, H. Kambara, N. Yoshimura, M. Hirata, T. Yoshimine, and Y. Koike, "Prediction of Three-Dimensional Arm Trajectories Based on ECoG Signals Recorded from Human Sensorimotor Cortex," *PLoS ONE*, vol. 8, no. 8, pp. 1-9, 2013.

[18] G. Onose, C. Grozea, A. Anghelescu, C. Daia, C. J. Sinescu, A. V. Ciurea, T. Spircu, A. Mirea, I. And one, A. Spanu, C. Popescu. A. -S. Mihaescu, S. Fazli, M. Danoczy, and F. Popescu, "On the feasibility of using motor imagery EEG-based brain-computer interface in chronic tetraplegics for assistive robotic arm control: a clinical test and long-term post-trial follow-up," *Spinal Cord*, vol. 50, pp. 599-608, 2012.

[19] I. Winkler, S. Haufe, and M. Tangermann "Automatic Classification of Artifactual ICA Components for Artifact Removal in EEG Signals," *Behav. Brain Funct.*, vol. 7, no. 30, pp. 1-15, 2011.

[20] A. Ziehe and K.-R. Müller, "TDSEP - an efficient algorithm for blind separation using time structure," Proceedings of the 8th International Conference on Artificial Neural Networks, Skövde, Sweden, pp. 675-680, 1998.

[21] D. Nguyen-Tuong, M Seeger, and J. Peters "Model Learning with Local Gaussian Process Regression," *Advanced Robotics*, vol. 23, no. 15, pp. 2015-2034, 2009.

[22] A. Aizerman, E. Braverman, and L. Rozonoer, "Theoretical foundations of the potential function method in pattern recognition learning," *Automation and Remote Control*, vol. 25, pp. 821-837, 1964.

[23] K.-R. Müller, C. W. Anderson, and G. E. Birch, "Linear and non-linear methods for brain-computer interfaces," *IEEE Trans. Neural Syst. Rehabil. Eng.*, vol. 11, no. 2, pp. 165-169, 2003.

[24] S. Lemm, B. Blankertz, T. Dickhaus, and K.-R. Müller, "Introduction to machine learning for brain imaging," *NeuroImage*, vol. 56, no. 2, pp. 387-399, 2011.

[25] J. M. Antelis, L. Montesano, A. Ramos-Mruguialday, N. Birbaumer, and J. Minguez, "On the Usage of Linear Regression Models to Reconstruct Limb Kinematics from Low Frequency EEG Signals," *PLoS ONE*, vol. 8, no. 4, pp. 1-14, 2013.

[26] S. Haufe, F. Meinecke, K. Görgen, S. Dähne, J.-D. Haynes, B. Blankertz, and F. Bießmann, "On the interpretation of weight vectors of linear models in multivariate neuroimaging," *NeuroImage*, 2013.

Jeong-Hun Kim received the BS degree in electronic engineering and avionics from Korea Aerospace University, Korea, in 2009 and the MS degree in brain and cognitive engineering from the Korea University, Seoul, in 2014. From 2009 to 2012, he worked at LG Electronics. His current research interests include machine learning and brain-computer interfaces.

Felix Bießmann obtained a BSc in Cognitive Science in 2005 from the University of Osnabrück, a MSc in Neuroscience at the International Max-Planck Research School, Tübingen, and a PhD in Machine Learning from Berlin Institute of Technology. His research interests include statistical learning methods for multimodal data with a focus on neuroscientific and biomedical data.

Seong-Whan Lee is a Hyundai Motor Chair Professor at Korea University, where he is the Head of the Department of Brain and Cognitive Engineering. He is a Fellow of the IEEE, IAPR, and Korean Academy of Science and Technology. His research interests include pattern recognition, computer vision, and brain engineering.